ISSN 2616-5767 Vol.6, Issue 6: 22-29, DOI: 10.25236/AJETS.2023.060604

Correction for a camera-projector 3D reconstruction system based on dithering fringe pattern

Xuexing Li[a,*], Jun Wang[b], Jie Zhu[c], Ningju Zhang[d]

School of Mechanical Technology, Wuxi Institute of Technology, Wuxi, China
[a]lixx@wxit.edu.cn, [b]Wangjun@wxit.edu.cn, [c]Zhujie@wxit.edu.cn, [d]Zhangnj@wxit.edu.cn
**Corresponding author*

Abstract: *The binary defocusing technique is widely used for high-speed three-dimension (3D) reconstruction. However, the system distortion directly influences the reconstruction quality, and most of the previous works are only for the traditional digital fringe projection (DFP) technique. Based on the problems above, this paper first analyzes the distortion for the input-output response of the system and the influence of space luminance distribution uniformity of the projector, in the binary defocusing technique. Then, a novel method combining initial correction and iterative correction is proposed to obtain accurate sinusoidal fringe patterns. Finally, the experimental results show that the proposed method can correct sinusoidal fringe phase error in binary defocusing technique significantly and improve the quality of 3D reconstruction effectively.*

Keywords: *3D reconstruction; Binary defocusing technique; System distortion; Distortion correction*

1. Introduction

The development of the digital fringe projection (DFP) technique has been made in high-quality three-dimension (3D) reconstruction thanks to the flexibility and simplicity of its system [1-4]. A series of sinusoidal fringe patterns generated by the computer are projected on an object by the project. Then, a camera captures the fringe patterns distorted by the object's surface geometry. Finally, the 3D shape of the object is reconstructed by fringe analysis algorithms. When a 3D reconstruction system is designed, it usually uses at least three sinusoidal phase-shifting fringe patterns, and these high-precision sinusoidal fringe patterns are easy to get since the liquid crystal display (LCD) or digital light processing (DLP) projector is developing. Unfortunately, there are nonlinear intensity responses caused by the projector-camera system, which lead to deviation of the output fringe from the ideal sinusoidal fringe [5].

In recent years, to reduce the influence of the nonlinear intensity responses, many correction methods have been proposed. Guo et al. [6] proposed a gamma-correction technique that applied the cumulative distribution function of sinusoidal signal to the estimation of the gamma. Zhang and Yau [7] proposed a correction method by creating a look-up table, and this method did not require the calibration of system gamma. Pan et al. [8] used a nonlinear function to depict the overall nonlinearity of a FPP system, and compensated the non-sinusoidal phase error by an iterative phase compensation algorithm. Baker et al. [9] proposed an appropriate model based on the harmonic structure of a gamma-distorted fringe. Zheng and Da [10] combined the two-step phase-shifting method with a pre-coding gamma correction method to attenuate the gamma distortion effect. Kakunai et al. [11] considered the nonlinear properties of the experimental system to compensate for locally varying reflectivity on the 3D profile by adjustment of the color component of the LCD projector. Huang et al. [12] proposed a simple phase error correction strategy with a polynomial fitting technique to suppress the nonlinear input-output response of a measurement system. There are two types of the methods above. In the first type, errors can be compensated by post-processing [6-10]. The second type is by adjusting the input fringe projector [11, 12]. Analyzing the methods above, we can find they just correct and compensates for the error of the system which is low-speed (even static) measurement as well as the continuous sinusoidal fringes inputted.

However, with recent trends in 3D reconstruction, the high-speed demand is growing [4]. Many novel high-speed reconstruction techniques have been proposed. The binary defocusing technique with a DLP projector is one of the most important technical means [13-19]. The technique pushes through the limitation that the maximum refresh rate of the conventional DFP technique only has 120 frame/s. The correction techniques [6-12] above cannot be used for the binary defocusing technology since its

ISSN 2616-5767 Vol.6, Issue 6: 22-29, DOI: 10.25236/AJETS.2023.060604

projection principle is different. Some researchers also pointed out that the binary defocusing technique can eliminate the nonlinear error of the projector [16-19]. However, this thesis is based on an assumption that the uniformity of space luminance distribution is captured by the camera. In practice, it is very difficult to guarantee.

In our paper, a method is proposed to conquer the challenges. This method includes two observations: (1) analyzing the distortion of the system: when the continuous gray patterns and dithering patterns are projected respectively, the distortion in the position of each pixel and the inference of space luminance distribution uniformity are analyzed, and (2) correcting the distortion of the system: we proposed a correction method (combine initial correction and iteration correction) to achieve the precise output sinusoidal patterns in binary dithering technique. Then, the experiments are presented to prove the effectiveness and accuracy of the proposed technique.

2. Principle

Phase-shifting algorithms have been extensively used in optical metrology. Especially, the three-step phase-shifting algorithm could achieve rapid measurement since it requires the minimum number of patterns to reconstruct the 3D profile [20]. In addition, when projecting the binary patterns, the DLP projector has an extremely high frame rate. Therefore, the researchers usually combine these two aspects to achieve real-time reconstruction performance. Fig. 1 shows a schematic experimental system for the phase-shifting method in this paper.

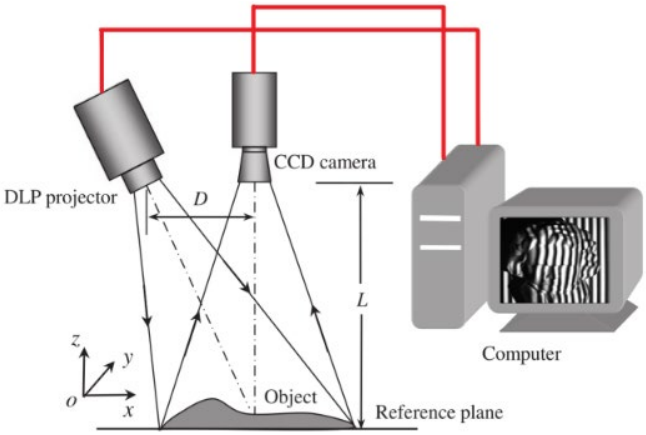

Figure 1: The experimental system of the phase-shifting method

2.1. System distortion

In Fig. 1, there are two major devices: a camera and a projector. The camera is commonly the industrial camera for measurement, and its correction has been completed in the factory. The projector is usually a commercial device, and it only gets the correction for the human eyes. Therefore, the distortion of the system is inevitable. In the following two sections, we analyze the system distortion.

2.1.1. Input-output gray distortion

Generally, to obtain a better visual effect, there is a nonlinear response (or gamma distortion) in the commercial projector. Theoretically, the gamma distortion model can be simply expressed as follows,

$$I_{out} = (I_{in})\gamma \tag{1}$$

where I_{out} is the output gray and I_{in} is the input gray. Exponent γ represents the gamma value. In recent studies, some researchers proposed the binary defocusing technique of a projector to eliminate nonlinear error. The result curve is similar to a proportional function. In other words, the binary defocusing technique can eliminate nonlinear errors. Theoretically, the relational expression can be simply expressed as follows,

$$I_{out} = aI_{in} + b \tag{2}$$

where the I_{out} and I_{in} are the same as the I_{out} and I_{in} in Eq. (1). The parameters a and b respectively represent the slope and intercept of linear representation.

ISSN 2616-5767 Vol.6, Issue 6: 22-29, DOI: 10.25236/AJETS.2023.060604

2.1.2. Space luminance distribution uniformity

As we all know, there are two kinds of image generation components in the general commercial projector: LCD and DLP, whose illumination sources are all the point light sources. In addition, the industrial camera is a photoelectric converting device that is much more sensitive to light than the human eyes. Therefore, the non-uniform luminance of the projector can be easily captured by the industrial camera to influence the output gray distribution. Fig. 2 shows the gray distribution captured by the camera when a pure white image is projected. In this Figure, the gray distributes as a mountain in the light area, and the mountaintop corresponds to the location of the point light source.

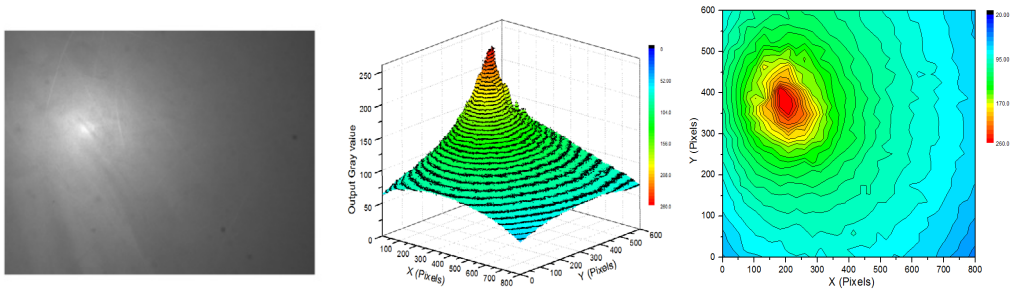

(a) (b) (c)

Figure 2: The response of a pure white input image. (a) The actual image. (b) The stereogram. (b) The height map.

In a word, considering all these two aspects above, (1) when the continuous gray images are projected, the gamma distortion (or nonlinear response) and gray non-uniform distribution are generated, and (2) when the binary images are projected, nonlinear error of projector has been eliminated, but the gray non-uniform distribution still exists.

2.2. Distortion correction

In this paper, we mainly study the binary sinusoidal pattern projection and its correction. The binary sinusoidal patterns are generated by the error-diffusion dithering technique, and its correction is realized by the following initial correction and iteration correction.

2.2.1. Initial correction

As described in Eq. (2), when the dithering images are projected and captured, the input and output gray represents a strong linear relation. Unfortunately, Eq. (2) only considers the uniform luminance rather than the non-uniform luminance of the point light source. Through the analysis of section 2.1.2, we know the point light source in the projector is very common. Thus, it may be suspected that the linear relationship is used in a non-uniform luminance distribution measurement system.

Next, we use the following steps to verify this suspect. It is necessary to note that to eliminate the influence of the environmental lights, the following works are finished in a dark room.

Step 1: The input images generated by the error-diffusion dithering technique are from 0 to 255, and sampled at intervals of 32. Then, these input images are projected by the projector, and the output images are captured by the camera, as shown in Fig. 3(a).

Step 2: Choose a cross-section [e.g. section I in Fig. 3(a)], which is perpendicular to the XOY plane, and then obtain the input and output relations on the section. For example, section I corresponds to Fig. 3(b).

Step 3: After the section choice, several points that have the same X coordinate on curves in Fig. 3(b) are marked, and these points have the same X coordinate. For example, we randomly selected four groups of points (black dots): l_1, l_2, l_3, and l_4, as shown in Fig. 3(b).

Step 4: Observing the black dots in each group, we can find the distance between the adjacent points is largely the same. That is to say, the input-output gray relationship curves of the black dots in the l_1, l_2, l_3, and l_4, groups are still strong linear, and their slopes and intercepts are shown in Table 1.

ISSN 2616-5767 Vol.6, Issue 6: 22-29, DOI: 10.25236/AJETS.2023.060604

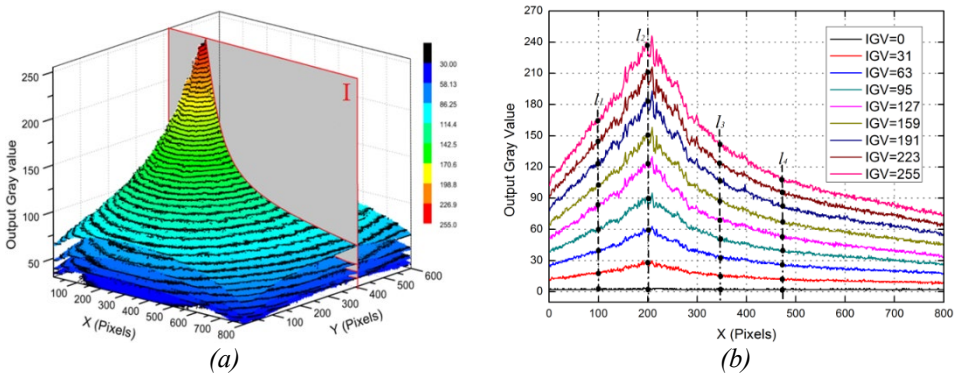

(a) (b)

Figure 3: The output gray distribution sequence at regular input gray interval (32 levels). (a) The stereogram. (b) A section of the sequence stereogram.

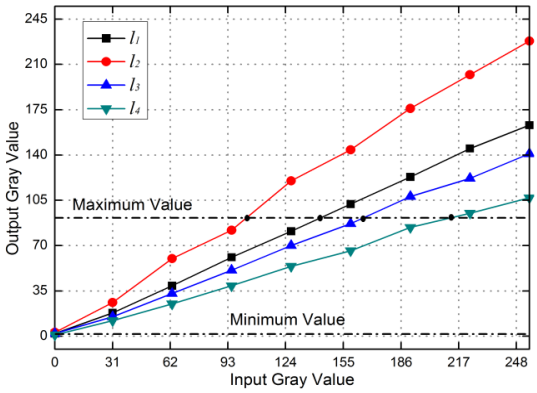

Figure 4: Input-output response curve

Table 1: The slopes and intercepts of the fitting lines in Fig. 4.

a	b
l1	0.6441
l 2	0.8988
l 3	0.5548

Through the analysis above, it is identified that the gray input-output relation of each pixel in the projection region is a strong linear relationship. Theoretically, the expression can be expressed as follows,

$$I_{out} = a(x, y)I_{in} + b(x, y), \tag{3}$$

where the I_{out} and I_{in} are the same as the I_{out} and I_{in} in Eq. (1) or (2). The parameter $a(x, y)$ and $b(x, y)$ respectively represent the slope and intercept of linear representation, but they are all the functions of pixel position, which is different from a and b in Eq. (2).

Based on the analysis of the above, we proposed an initial correction method which is to use the inverse function of Eq. (3), as expressed in Eq. (4).

$$I'_{in} = \frac{I'_{out} - b(x, y)}{a(x, y)} \tag{4}$$

where the value range of I'_{in} is 0 to 255, and the value range of I'_{out} needs to be defined with the rules: (1) the minimum value of I'_{out} should be bigger than the maximum value of each pixel when the pure black is input, and (2) the maximum value of I'_{out} should be smaller than the minimum value each pixel when the pure white image is input. That is, the purpose of the two rules above is to make the gray value I'_{out} of each pixel with the same value range. As shown in Fig. (4), the maximum value line and minimum value line limit the value range of I'_{out}, which is also the bound of the ideal sinusoidal pattern. In addition, the $a(x, y)$ and $b(x, y)$ in Eq. (4) are different in each pixel. However, when the system is built, the $a(x, y)$ and $b(x, y)$ are also determined. We can utilize the steps above to solve the $a(x, y)$ and $b(x, y)$ each pixel, and the non-sampled pixels can be solved by the linear interpolation, as shown in Fig.

ISSN 2616-5767 Vol.6, Issue 6: 22-29, DOI: 10.25236/AJETS.2023.060604

(5).

In a word, the purpose of the initial correction is to obtain the input image by Eq. (4), and the input images are projected by a projector to get the output images which are similar to the ideal sinusoidal pattern. Fig. 6(a) and Fig. 6(b) respectively show the ideal sinusoidal pattern and uncorrected output pattern. However, as shown in Fig. 6(c), the initial correction method only corrects most of the differences between the ideal pattern and the output pattern captured by a camera. The main cause of this problem is that there is a defocusing step in the process of projection. Projector defocusing could create a smoothing effect towards the image which can be modeled as a Gaussian filter. Thus, a pixel can be influenced by its neighboring pixels when the projector is defocusing. For example, in the Error-diffusion dithering algorithm, the pixel P_0 could be influenced by its neighboring pixels P_1, P_2, P_3 and P_4, as shown in Fig. 7(a). When the parameters $a(x, y)$ and $b(x, y)$ in the initial correction are calculated, we input the pure gray images after dithering. As shown in Fig. 7(b), the pixel T_0 is influenced by T_1 and T_2. The pixel T_0, T_1 and T_2 are required the same output gray. However, in practice the output gray of the pixel Q_0, Q_1 and Q_2 in sinusoidal fringe are different, as shown in Fig. 7(c). Therefore, the parameters $a(x, y)$ and $b(x, y)$ in the initial correction do not fully correct the dithering sinusoidal fringe patterns.

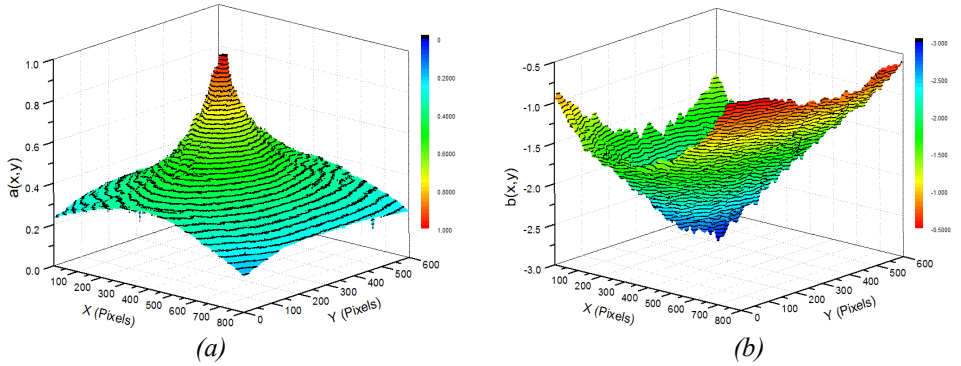

Figure 5: The slop a(x, y) distribution and intercept a(x, y) distribution of each pixel. (a) The a(x, y) distribution. (b) The a(x, y) distribution.

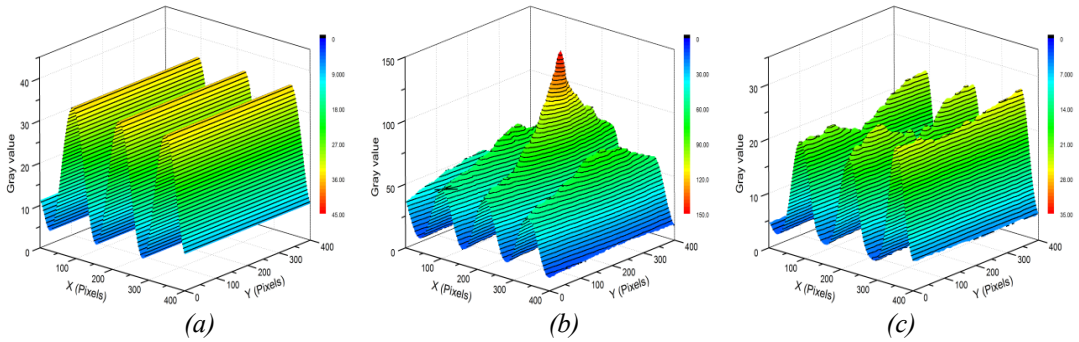

Figure 6: The diagrams of initial correction. (a) The ideal sinusoidal pattern. (b) The uncorrected output pattern. (c) The output pattern by initial correction.

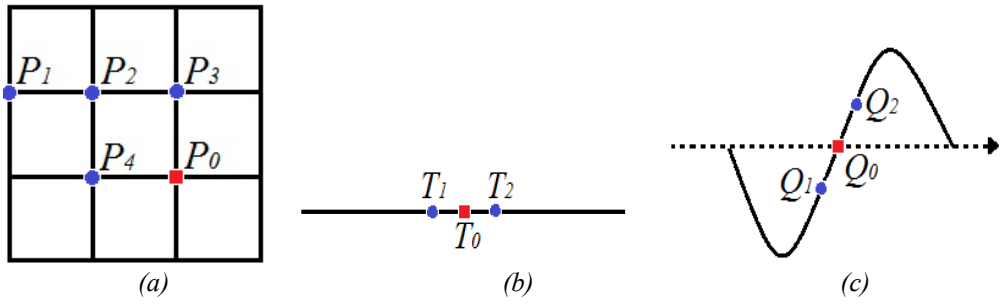

Figure 7: The diagrams of defocusing. (a) The defocusing of error-diffusion dithering algorithm. (b) The defocusing in initial correction. (c) The defocusing in practice.

ISSN 2616-5767 Vol.6, Issue 6: 22-29, DOI: 10.25236/AJETS.2023.060604

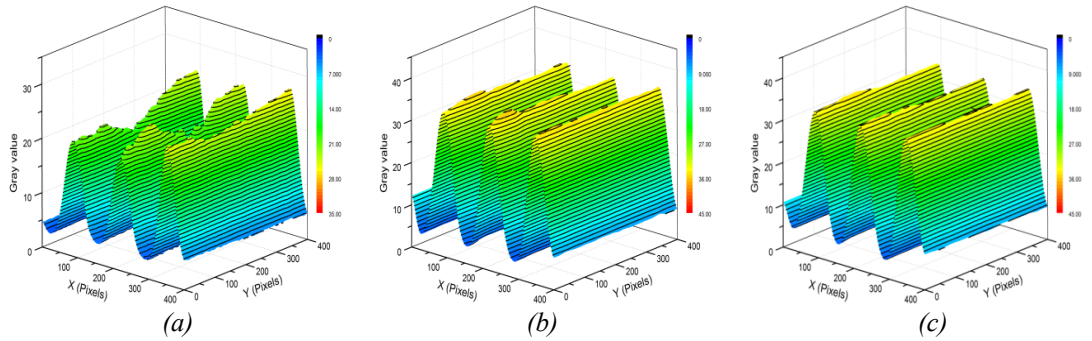

Figure 8: The diagrams of iteration correction. (a) The pattern after initial correction. (b) The pattern processed by 3 times iteration correction. (c) The pattern processed by 5 times iteration

2.2.2. Iteration correction

The initial correction above has finished most of the correction, and then we also proposed an iteration correction method to complete the rest of the accurate error correction.

Step 1: The initial correction above has obtained the iteration beginning conditions, i.e., the beginning input pattern $I'_{in,(0)}$ and the beginning output pattern $I'_{out,(0)}$.

Step 2: Eq. (5) is the proposed iteration relation, which loops iteration several times to get the accurate pattern in the final output.

$$\left[I'_{ideal} - I'_{out,(k)}\right] + I'_{in,(k)} = I'_{in,(k+1)}, (k = 0,1,2,\cdots,n), \tag{5}$$

where the pattern I'_{ideal} represents an ideal sinusoidal pattern, which is an iteration's goal. The pattern $I'_{out,(k)}$ and $I'_{in,(k)}$ respectively represent the output and input pattern of the system in the current iteration, and the pattern $I'_{in,(k+1)}$ represents the input pattern of the system in the next iteration. In Eq. (5), $\left[I'_{ideal} - I'_{out,(k)}\right]$ is as a compensation amount in iteration, and $I'_{out,(k)}$ gradually tends to the ideal target pattern.

We propose two convergence rules: (1) if the system only has the minor defects of non-uniform brightness, the intensity RMS error difference for a new round of iterations is required to be less than 0.1%, and (2) if the system has the major defects of non-uniform brightness, the iterative times (10 to 15) is required since the major defects normally are difficult to be corrected the error that is less than 0.1%.

In Fig. 8, there is an example of iteration correction. Fig. 8(a) show the pattern after initial correction. Fig. 8(b) show the pattern processed by iteration correction (k=3 times). Fig. 8(c) show the pattern processed by iteration correction (k=5 times). Obviously, with the number of iterations, the rest of the accurate error goes down.

3. Experiments

The proposed correction algorithm is verified by a fringe projection system, the theory diagram as shown in Fig. 1 and the actual experiment environment as shown in Fig.9. In Fig. 9, the devices include a DLP projector (Model: Vivitek D555WH) with 1024×768 native resolution, a change coupled device (CCD) camera (Model: DALSA DS-24-02M30) with 800×600 resolution, and two computers which are used to project and acquire respectively. The camera was attached with a 25mm focal length Mega-pixel lens (Model: Wowa LM25HC) with F/1.4 to 16 C-Mount. The distance between the camera and projector is about 20 cm and the distance between the camera and the reference plane is about 80 cm. We complete two experiments: (1) the tested object is a white plane, and (2) a cross-shaped foam model, as shown in Fig. 10. It is necessary to note that the experiments are completed in a dark room.

Test 1: The tested object is a white plane. At first, through the proposed initial correction method, the parameter $a(x, y)$ and $b(x, y)$ under the current experimental condition are determined, and then the input patterns which can compensate the most of the error are obtained. Next, each input pattern after initial correction is processed by the processed iteration correction method. In this test, pattern adaptation is iterated 10 times. Fig. 11 shows a row in unwrap phase of output patterns. Obviously, in comparison with the uncorrected result, the quality of the corrected result is much better, and the standard deviations of

ISSN 2616-5767 Vol.6, Issue 6: 22-29, DOI: 10.25236/AJETS.2023.060604

the phase error are 0.3862 rad and 0.0938 rad respectively.

Test 2: The tested object is a cross-shaped foam model. The phase-shifting fringe patterns generated in Test 1 are projected on a cross-shaped foam model. The fringe patterns are distorted by the object, and then its 3D shape is reconstructed by the three-step phase-shifting algorithm [20]. Fig. 12 shows the 3D point cloud of the object. It can be seen that the phase measuring performance is highly improved.

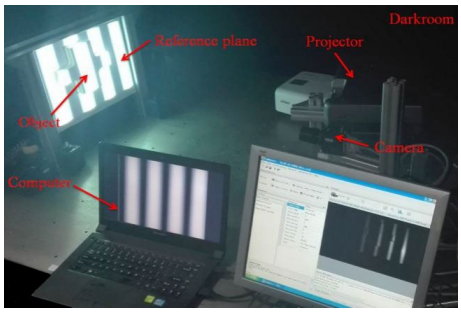

Figure 9: The actual experiment environment

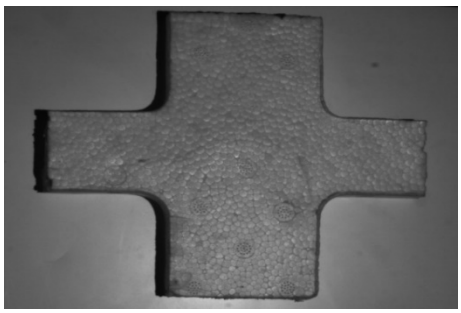

Figure 10: A cross-shaped foam model.

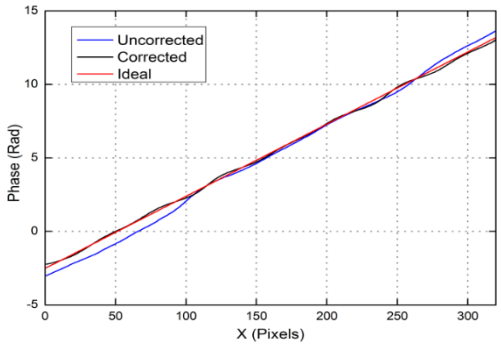

Figure 11: A row in unwrap phase of output patterns.

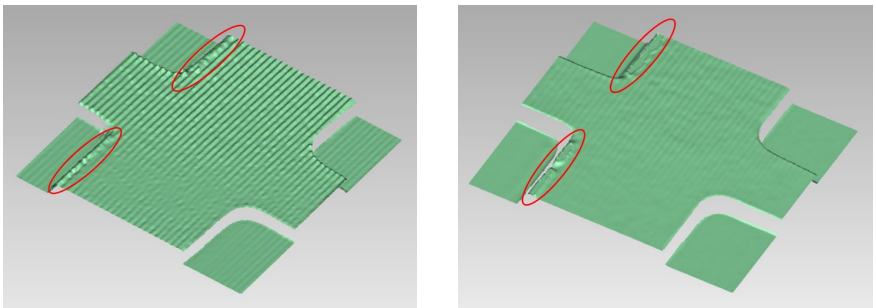

(a) *(b)*

Figure 12: 3D point cloud. (a) Uncorrected. (b) Corrected. Note: The quality of the regions circled by red is poor since they are the shadow area in the measurement

ISSN 2616-5767 Vol.6, Issue 6: 22-29, DOI: 10.25236/AJETS.2023.060604

4. Conclusion

This paper has presented a correction method for binary defocusing technique. This method, which considered the distortion of the input-output response of the system and the inference of space luminance distribution uniformity projected in binary defocusing technology, obtained the accurate output sinusoidal patterns by steps of initial correction and iterative correction. Experimental results showed that the method is efficient. The sinusoidal quality is highly improved for binary fringe projection systems; thus, high-quality phase measurement can be achieved.

Acknowledgements

This research was funded by the Natural Science Foundation of the Jiangsu Higher Education Institutions of China, grant number 21KJB460026, the industry-university-research Cooperation Project of Jiangsu Province, grant number BY2021245, Wuxi Soft science research subject, grant number KX-22-C233.

References

[1] Yu X., Liu Y. K. and Liu N. Y. (2019) NFlexible gamma calculation algorithm based on probability distribution function in digital fringe projection system. Health, 27, 32047-32057.
[2] Li X. X., Zhang W. H. (2021) Phase error analysis and compensation for motion in high-speed phase measurement profilometry. Health, 4, 1191-1206.
[3] Wang J. H., Yang Y. X. (2022) Phase extraction accuracy comparison based on multi-frequency phase-shifting method in fringe projection profilometry. Health, 199, 111525.
[4] Li X. X., Zhang Z. J. and Yang C. (2016) High-quality fringe pattern generation using binary pattern optimization based on a novel objective function. Health, 127, 5322-5327.
[5] Gorthi S. S., Rastogi P. (2010) Fringe projection techniques: whither we are? Health, 48, 133-140.
[6] Guo H. W., He H. T. and Chen M. Y. (2004) Gamma correction for digital fringe projection profilometry. Health, 43, 2906-2914.
[7] Zhang S., Yau S. T. (2007) Generic nonsinusoidal phase error correction for three-dimensional shape measurement using a digital video projector. Health, 46, 36-43.
[8] Pan B., Kemao Q., Huang L. and Asundi A. (2009) Phase error analysis and compensation for nonsinusoidal waveforms in phase-shifting digital fringe projection profilometry. Health, 34, 416-418.
[9] Barker M. J., Xi J. T., Chicharo J. F. (2008) Elimination of gamma non-linear luminance effects for digital video projection phase measuring profilometers, in: Proceedings of IEEE Conference on Electronic Design, Test and Applications (IEEE), pp. 496-501.
[10] Zheng D. L., F. P Da (2011) Gamma correction for two step phase shifting fringe projection profilometry. Health, 124, 1392-1397.
[11] Kakunai S., Sakamoto T. and Iwata K. (1999) Profile measurement taken with liquid-crystal gratings. Health, 38, 2824-2828.
[12] Huang P. S., Zhang C. and Chiang F. P. (2003) High-speed 3-D shape measurement based on digital fringe projection. Health, 42, 163-168.
[13] Lei S. Y., Zhang, S., Flexible 3-D shape measurement using projector defocusing. Health, 34 (2009) 3080-3082.
[14] Ayubi G. A., Ayubi J. A., Martino J. M. Di and Ferrari J. A. (2010) Pulse-width modulation in defocused three-dimensional fringe projection. Health, 35, 3682-3684.
[15] Wang Y., Zhang S., (2010) Optimal pulse width modulation for sinusoidal fringe generation with projector defocusing. Health, 35, 4121-4123.
[16] Lohry W., Zhang S. (2012) 3D shape measurement with 2D area modulated binary patterns. Health, 50, 917-921.
[17] Wang Y. J., Zhang S. (2012) Three-dimensional shape measurement with binary dithered patterns. Health, 51, 6631-6636.
[18] Li B. W., Wang Y. J., Dai J. F., Lohry W. and Zhang S. (2014) Some recent advances on superfast 3D shape measurement with digital binary defocusing techniques. Health, 54, 236-246.
[19] Lohry W., S. Zhang S. (2013) Genetic method to optimize binary dithering technique for high-quality fringe generation. Health, 38, 540-542.
[20] You D., You Z. S., Zhang X. and Zhu J. P. (2022) High-quality 3D shape measurement with binary half truncated sinusoidal fringe pattern. Health, 155, 107046.